In situ mapping of biomineral skeletal proteins by molecular recognition imaging with antibody-functionalized AFM tips

Benazir Khurshid, Eric Lesniewska, Luca Polacchi, Maëva L'Héronde, Daniel J. Jackson, Sébastien Motreuil, Jérôme Thomas, Jean-François Bardeau, Stephan E. Wolf, Daniel Vielzeuf, et al.

To cite this version:

Benazir Khurshid, Eric Lesniewska, Luca Polacchi, Maëva L'Héronde, Daniel J. Jackson, et al.. In situ mapping of biomineral skeletal proteins by molecular recognition imaging with antibody-functionalized AFM tips. Acta Biomaterialia, 2023, 168, pp.198-209. 10.1016/j.actbio.2023.07.028 . hal-04272655

HAL Id: hal-04272655
https://hal.science/hal-04272655

Submitted on 6 Nov 2023

Acta Biomaterialia

In situ mapping of biomineral skeletal proteins by molecular recognition imaging with antibody-functionalized AFM tips

--Manuscript Draft--

Manuscript Number:	AB-23-620R2
Article Type:	Full length article
Keywords:	biominerals; molluscan shell; skeletal matrix; molecular recognition; Atomic force microscopy; antibody
Corresponding Author:	Frederic MARIN, PhD, Habil. University of Bourgogne Dijon, France
First Author:	Benazir Khurshid, Ph.D
Order of Authors:	Benazir Khurshid, Ph.D
	Eric Lesniewska
	Luca Polacchi
	Maëva L'Héronde
	Daniel J. Jackson
	Sébastien Motreuil
	Jérôme Thomas
	Jean-François Bardeau
	Stephan E. Wolf
	Daniel Vielzeuf
	Jonathan Perrin
	Frederic MARIN, PhD, Habil.
Abstract:	Spatial localizing of skeletal proteins in biogenic minerals remains a challenge in biomineralization and biomaterials research. To address this goal, we developed a novel in situ mapping technique based on molecular recognition measurements via atomic force microscopy (AFM). In order to obtain 2D maps of the distribution of a specific protein, three steps are required (1) the development and purification of a polyclonal antibody elicited against the target protein, (2) its covalent coupling to a silicon nitride AFM tip ('functionalization'), and (3) scanning of an appropriately prepared biomineral surface. We applied this approach to a soluble molluscan shell protein - accripin11 - recently identified as a major component of the calcitic prisms of the fan mussel Pinna nobilis [1]. Multiple tests reveal that accripin11 is evenly distributed at the surface of the prisms but is also present in the organic sheaths surrounding the calcitic prisms, which indicates that accripin11 is both an intra- and inter-crystalline protein. We also observed that the adhesion force in transverse sections is about twice higher than in longitudinal sections, suggesting that the protein is not randomly oriented in the biomineral but may exhibit preferred orientation. To our knowledge, this is the first time that a protein is localized by molecular recognition atomic force microscopy with antibody-functionalized tips in a biogenic mineral. The 'pros' and 'cons' of this new methodology in the biomineralization field are discussed in comparison with more 'classical' approaches like immunogold localization. This technique, which leaves the surface to analyze clean, might prove useful for clinical tests, on non-pathological (bone, teeth) or pathological (kidney stone) biomineralizations. Studies using implants with protein-doped calcium phosphate coating can also benefit from this technology.

Graphical Abstract

Mapping of a shell protein by AFM with antibody-functionalized tip

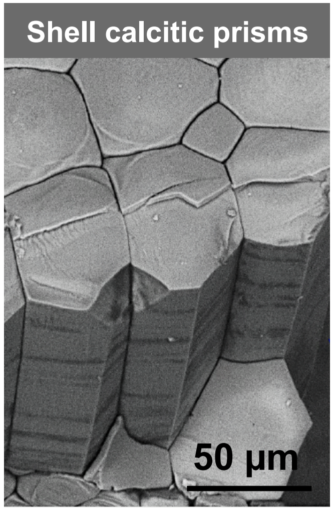

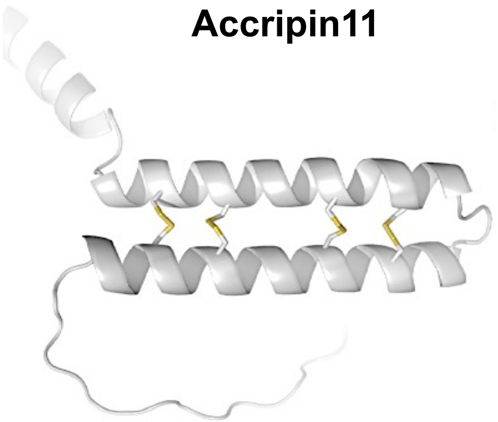

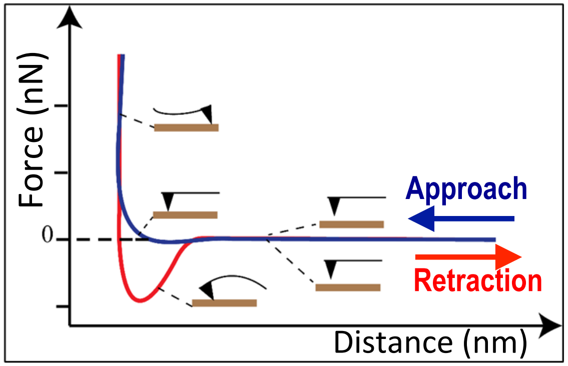

Principle of Single-Molecule-Force-Spectroscopy

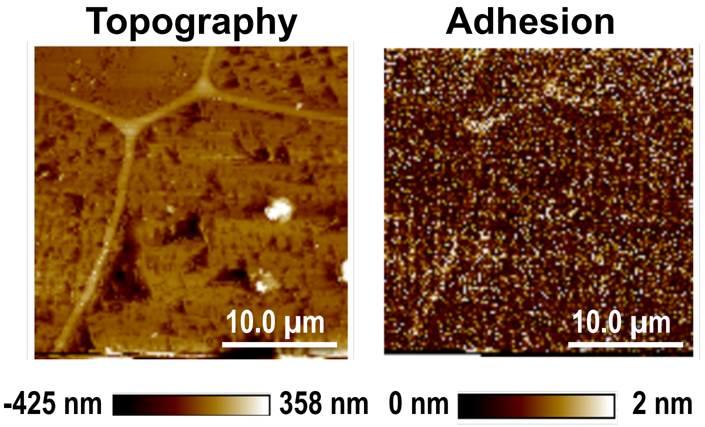

In situ mapping of biomineral skeletal proteins by molecular recognition imaging with antibody-functionalized AFM tips

Benazir Khurshid[1,2], Eric Lesniewska[3], Luca Polacchi[4,5], Maëva L'Héronde[4], Daniel J. Jackson[6], Sébastien Motreuil[1], Jérôme Thomas[1], Jean-François Bardeau[7], Stephan E. Wolf[8], Daniel Vielzeuf[9], Jonathan Perrin[2], Frédéric Marin[1*]

Authors affiliations :

[1] Laboratoire Biogéosciences, UMR CNRS-EPHE 6282, University of Burgundy, Dijon, France.

[2] Synchrotron SOLEIL, Beamline ANATOMIX, Saint-Aubin, Gif-sur-Yvette, France.

[3] Laboratoire Interdisciplinaire Carnot de Bourgogne (ICB), UMR CNRS 6303, University of Burgundy, Dijon, France.

[4] IPANEMA, USR3461, CNRS/MCC, Saint-Aubin, Gif-sur-Yvette, France.

[5] CR2P UMR7207, Muséum National d'Histoire Naturelle, Paris, France.

[6] Department of Geobiology, Georg-August University of Göttingen, Göttingen, Germany.

[7] IMMM UMR CNRS 6283, Le Mans University, Le Mans, France.

[8] Institute of Glass and Ceramics, Dpt. Materials Science & Engineering, Friedrich-Alexander-University, Erlangen, Germany.

[9] CINAM, Aix Marseille University, CNRS, Marseille, France.

[*] Corresponding author: Frédéric Marin: frederic.marin@u-bourgogne.fr

Abstract

Spatial localizing of skeletal proteins in biogenic minerals remains a challenge in biomineralization research. To address this goal, we developed a novel *in situ* mapping technique based on molecular recognition measurements via atomic force microscopy (AFM), which requires three steps: (1) the development and purification of a polyclonal antibody elicited against the target protein, (2) its covalent coupling to a silicon nitride AFM tip ('functionalization'), and (3) scanning of an appropriately prepared biomineral surface. We applied this approach to a soluble shell protein - accripin11 - recently identified as a major component of the calcitic prisms of the fan mussel *Pinna nobilis* [1]. Multiple tests reveal that accripin11 is evenly distributed at the surface of the prisms and also present in the organic sheaths surrounding the calcitic prisms, indicating that this protein is both intra- and inter-crystalline. We observed that the adhesion force in transverse sections is about twice higher than in longitudinal sections, suggesting that accripin11 may exhibit preferred orientation in the biomineral. To our knowledge, this is the first time that a protein is localized by molecular recognition atomic force microscopy with antibody-functionalized tips in a biogenic mineral. The 'pros' and 'cons' of this methodology are discussed in comparison with more 'classical' approaches like immunogold. This technique, which leaves the surface to analyze clean, might prove useful for clinical tests on non-pathological (bone, teeth) or pathological (kidney stone) biomineralizations. Studies using implants with protein-doped calcium phosphate coating can also benefit from this technology.

Keywords: biomineral, protein mapping, AFM, molluscan shell, skeletal matrix, molecular recognition, antibody

1. Introduction

Biogenic calcium carbonates are the most abundant components of biominerals in nature [2]. They are also phylogenetically widespread across the Tree of Life [3], being produced by bacteria and protists and most metazoan phyla including sponges, cnidarians, bryozoans, brachiopods, molluscs, annelids, arthropods, echinoderms and some vertebrates, among which birds (eggshell) or teleost fishes (otoliths). Biominerals exhibit mechanical, textural, morphological or optical properties that are significantly different from their inorganic counterparts. Consequently, they present many avenues of exploration, from biomaterials science to bio-inspired chemistry and biomimicry [4-7]. In many aspects, the molluscan shell is considered as the archetypal example of a calcium carbonate biomineral for its remarkable resistance to fracture [8], the variety of crystal shapes that constitute each shell layer [9] and in some cases, its remarkable optical properties [10, 11]. These uncommon features are often considered as the result of non-classical crystallization pathways [12-16], themselves largely driven by the interaction of organic macromolecules with inorganic ionic precursors (*e.g.* calcium and carbonate/bicarbonate). The macromolecules secreted by the calcifying mollusc mantle at the mineral growth front may play multiple roles in the poorly understood transition from the initial crystallizing medium to the final calcified product. They are often occluded within the mature biomineral [17, 18].

While the functional mechanisms by which organic macromolecules influence the form of the mature biomineral are yet to be fully described, many studies have been carried out to identify and characterize these macromolecules, comprised predominantly of both proteins and polysaccharides [17, 19]. Only the first ones have received the greatest attention due to classical molecular biology approaches and to the rise of 'omics' techniques (*i.e.*, genomics, transcriptomics and proteomics) in recent years. The shell proteome, also defined as the "shellome" (*i.e.*, the set of proteins associated directly with the shell [20]) of dozens of mollusc species have now been characterized, at least partially [21, 22]. Many of these shell proteins do not have clear homologues in other model systems, and thus their precise function in biomineralization is largely unknown. To address this question, a variety of approaches are taken, which include: 1) *in silico* analyses of the protein sequence, accompanied by similarity search emphasizing functionally conserved domains; 2) adequate *in vitro* functional assays of recombinantly expressed versions of the target protein; 3) the "wet-lab" resolution of their 3D structures (via NMR studies of the crystallized proteins); 4) the knock-down of their corresponding transcripts via RNAi methods, or their knock-out (or modification) via CRISPR/Cas9 gene editing; 5) and finally, the precise *in situ* localization of the target protein within the biomineralized structure.

Mapping the distribution of a specific shell protein with a high spatial resolution is a necessary step to understand its affinity and its interactions with the mineral phase, and ultimately, its function during the liquid-solid transition [12-14]. However, what may appear as trivial is singularly complicated by the nature of the material, in particular its multiscale structure and the heterogeneity of the associated organic matrix. Only techniques with high resolution can overcome these limitations. In that respect, Atomic Force Microscopy (AFM) is a powerful tool in nano characterization because of its ability to scan a surface with subnanometer resolution in air and under vacuum but also in aqueous liquids. Apart from being used as an imaging tool, AFM rapidly became a multifunctional toolbox [23-27]. In biomineralization, AFM has been used to observe the ultrastructure of various shells [28-30]. Recently, a significant improvement was brought to the AFM technique by combining AFM imaging with the force measurement, known as molecular recognition imaging [31], also defined as Force Distance (FD)-based AFM. This technique relies on the interaction between two molecules: one is covalently attached to the AFM tip while the other, the target molecule, is bound to the surface of interest. Approaching the functionalized tip to the target molecule allows measuring the interaction force between the two molecules. The technique has a great sensitivity at the piconewton scale [32, 33] and the operation can be performed on multiple independent spots of the surface. Alternatively, the surface can be scanned continuously, line after line, with the functionalized tip. This allows a complete 3D map to be formed where each pixel is characterized by its corresponding adhesion curve. In parallel, a direct correlation between the topography of a sample, with structurally localized mechanical properties, and a specific interaction map can be obtained [34]. So far, molecular recognition imaging has been used on a variety of biomolecular systems, including antigen-antibody complexes [35, 36], aptamer-protein [37], peptide-protein [38], chromatin [39], cells [40, 41], and other ligand-receptor interactions such as avidin-biotin [42]. However, to our knowledge, this approach has never been applied to the surface of biominerals.

In this study, we performed AFM molecular recognition imaging of a newly discovered shell protein, accripin11 [1] in the calcitic prisms of the Mediterranean fan mussel, *Pinna nobilis*. The AFM probe was functionalized with a highly specific and purified polyclonal antibody, which was elicited against two peptides of this protein. The probe was subsequently used to scan two orthogonal surfaces of the calcitic prisms. With this approach, we successfully obtained a distribution map of accripin11. The pros and cons of the technique are discussed here.

2. Materials and methods

2.1. Materials sampling - Ten fresh shells of the Mediterranean fan mussel *Pinna nobilis*, a highly protected species, were collected during a field mission in May 2017. The mission was done according to ethical rules. In particular, the sampling required a specific authorization of the DDTM ('Direction Départementale du Territoire et de la Mer' of the department of Alpes Maritimes, Arrêté Préfectoral n° 2017-459). All the metadata describing the mission can be accessed via the dat@UBFC portal of the Observatoire des Sciences de l'Univers (OSU) Theta, Besançon, France at: https://search-data.ubfc.fr/search.php?s=Pinna+nobilis.

2.2. Material microstructural description – *P. nobilis* exhibits a shell that consists of two superimposed layers (Figure 1a): the internal lustrous shell layer, which is restricted to the first third of the shell, is made of row stack nacre tablets of aragonite; the external brown-reddish layer exhibits a very characteristic pattern, consisting of large calcitic prisms that are packed within a honeycomb organic network, corresponding to the dark outlines observed in Figure 1b. This network forms insoluble sheaths around each single prism adhering them together. The prisms grow inwards, ‘layer-per-layer', perpendicularly to the outer shell surface (blue arrow in Figure 1b). If the isolated prismatic layer is treated with sodium hypochlorite, it can be entirely dissociated into 'single prisms', as shown by Figure 1c. In this study we only considered the prismatic layer, allowing us to focus on the *in situ* localization of a 'model' protein with functionalized AFM tips.

2.3. Choice of a model protein for *in situ* localization experiments - Our investigations on the protein composition of the prisms, combining transcriptomics and proteomics, led to the identification of hundreds of proteins (Khurshid *et al.*, in preparation). We selected one candidate, the sequence of which was extremely well covered by proteomics. In addition, it proved to be very abundant in the prisms and specific to this microstructure. We named this novel protein accripin11 and its biochemical properties have been recently described [1]. In short, accripin11 is a secreted protein of 103 amino acid residues (121 residues with signal peptide). It is moderately acidic, except at its C-terminus, enriched in 10 acidic residues (between positions 105 and 121) among which 7 are Asp residues (figure 2a). The protein exhibits a peculiar cysteine pattern in its central domain. In computerized 3D reconstructions using AlphaFold2, this pattern constrains the 3D structure to two antiparallel alpha-helices that are stabilized by four disulfide bridges. The acidic C-terminus is unstructured, *i.e.*, disordered (Figure 2b). Since accripin11 does not exhibit homology with any proteins of known function, its molecular role in the prism’s formation remains enigmatic; beyond being able to modify the shapes of calcite crystals *in vitro* [1], we suggest that accripin11 can act as a linker between the mineral surface and other matrix proteins: the Asp-rich C-terminus would bind the positively charged surface of growing calcium carbonate nuclei via electrostatic interactions while the more hydrophobic domain, containing the two antiparallel alpha-helices would be repelled and protrude from the surface, being able to bind other matrix protein partners. In the present localization experiments, accripin11 constitutes our model protein.

2.4. Polyclonal antibody production, testing and purification – In our previous paper [1], a recombinant accripin11 was obtained in insufficient amounts for developing functional assays and, in parallel, raising antibodies. Consequently, while most of the recombinant protein was utilized for functional assays, the following procedure was performed by Eurogentec SA (Liège Science Park, Seraing, Belgium) to generate polyclonal antibodies, according to the protocol called the “double X option”: in short, two immunogenic peptides were designed and synthesized: the first corresponding to the central domain (KDCAQQCTRDRETCFG, residues 65 to 80); the second to the C-terminal region (TAAPKPAKEPSSADD, residues 97 to 111) as shown by the two domains underlined in brown and in grey of Figure 2a. These peptides were coupled to carriers (KLH for the first peptide, and OVA for the second) and injected into rabbits, to generate polyclonal antibodies according to a speedy 28-day immunization protocol (contract FR10162), including injections at 0, 7, 10 and 18 days, and bleedings at 0 (pre-immune serum), 21 (medium), and 28 (final) days. The sera (2nd and 3rd bleeding) containing the antibodies were tested by Enzyme linked ImmunoSorbent Assay (ELISA) against the whole acetic acid soluble prism matrix, for the determination of their respective titer. In parallel, they were tested on Western blot against the same prism extracts to check their specificity [1].

Following the results of the Western blot, we selected the 3rd bleed serum, which was found to combine both high titer and high specificity. The antibodies were purified from their serum by an antibody purification kit (ref. ab109209, Abcam France, Paris) based on the binding of antibodies (*i.*e, immunoglobulins) to Protein A fixed to resin beads. The purification was performed according to the manufacturer's instruction: the serum containing the antibodies was mixed, first with the 10x binding buffer, then with the Protein A resin, and the mixture was incubated for 3 hours at room temperature with gentle agitation on a rotary shaker, to optimize binding of the antibody to the Protein A grafted resin. The suspension was poured and packed in a separating column, which was washed 3 times with 7 mL of washing solution to elute unbound serum macromolecules (including proteins), metabolites and inorganic ions contained in the serum. The antibody was then eluted and collected in a 2 mL Eppendorf tube by pouring 1 mL elution buffer in the column. This operation was repeated five times in total, each time with a new Eppendorf tube. 0.25 mL neutralizing buffer was added and mixed immediately to each of the 5 collected eluents. The 5 preparations were then placed on ice before testing.

Aliquots (20 μL) of the five eluents were then sampled, mixed to 20 μL of 2x Laemmli buffer, heat-denatured for 5 min., and tested on a 12% acrylamide hand cast SDS-PAGE gel, as previously described [43]. The gel was stained with silver nitrate [44]. In parallel, a second identical gel was electro-blotted on nitrocellulose according to the standard Western blot protocol [45]. As the antibody preparation (IgGs) cross-reacts with the secondary antibody (*i.e.*, GAR/AP, Sigma-Aldrich A3687), the membrane was then simply blocked with gelatin (0.5% wt/vol. in Tris buffered saline) and treated directly with GAR/AP (diluted 30,000 times), before being rinsed five times with TBS/Tween, revealed with NBT/BCIP and dried. The Eppendorf tubes containing the highest concentration of antibodies were pooled together and this solution was dialyzed (SpectraPor 7, cutoff 1 kDa) against 2L ultrapure water, with two water changes, in order to remove the salt of the neutralizing buffer, which may interfere with subsequent AFM tip functionalization. The solution was further concentrated in a Vivaspin 20 mL centrifugal concentrator tube (Sartorius, Germany, ref. VS2002, cutoff 10 kDa) to a final volume of 1.5 mL (3 times concentration) and stored at 4°C for quick use, or aliquoted and frozen for long term storage.

2.5. Functionalization strategy - The strategy for functionalizing AFM tips relies on the covalent binding of the antibody to the silicon nitride tip, as shown in Figure 3. We used a direct coupling procedure known as the 'glutaraldehyde pathway' [46-48], which does not require intermediate linker ('spacer') like polyethyleneglycol (PEG) [49]. The pathway is a four-step procedure, interspersed with short rinsing steps. The first step is the silanization, required to activate the tip by introducing amine groups. The interest of this step is that the probe can be functionalized directly, without prior surface preparation [50]. The silanization reaction occurs between silanol groups of the tip surface and a trichlorosilane group in the silane reagent, leading to the formation of an organosilane layer [51]. The second step is the glutaraldehyde incubation, which substitutes active aldehyde groups to amines of the APTES modified surface. In the third step, the antibody covalently binds to the active aldehyde groups [52]. In the last step, bovine serum albumin (BSA) blocks the remaining active sites where the antibody is not present.

2.6. AFM tip functionalization - We used silicon nitride AFM tip (ScanAsyst-Air probe with a nominal spring constant of 0.4 N/m, Bruker Nano). The functionalization was performed according to the protocol described in [52]. All steps were performed at room temperature. The tip was first silanized with 2% v/v 3-aminopropyltiethoxysilane (APTES, ref. 440140-100ML, Sigma-Aldrich) in acetone (ACS reagent, ref. 179124-500 ML, Sigma-Aldrich) for 10 minutes to render the AFM probe NH_2-activated. The AFM tip was then briefly rinsed with ultrapure water and immersed for 30 min. in glutaraldehyde (grade II, ref. G6257-100ML, Sigma-Aldrich) solution (0.5% v/v glutaraldehyde in ultrapure water). The tip was again rinsed with ultrapure water and incubated in a solution of purified anti-accripin11 antibody (200–300 ng/µl) for 30 min, before being briefly rinsed in ultrapure water. Finally, the remaining aldehyde groups on the probe surface were blocked by treating the tip for 1 min with 100 µg/L bovine serum albumin (BSA, 25 g, ref. RPN412V, GE Healthcare), filtered sterile (0.22 µm) in Tris buffered saline (TBS). The functionalized tip was stored in phosphate buffered saline (PBS) at 4°C or immediately mounted on the AFM tip holder for scanning.

2.7. Sample surface preparation for AFM study - We prepared two prismatic shell surfaces, each orthogonal to the other: transversal sections perpendicular to the elongation axis of the prisms; and longitudinal sections parallel to their elongation axis. These preparations were realized by using an ultramicrotome for obtaining flat, freshly exposed, surfaces. To this end, we used a Leica EM UC6 ultramicrotome (Leica, Austria), available at IPANEMA laboratory, Gif-sur-Yvette, France. First, the sample was cut by means of a wire saw (Well Diamond Wire Saws, model 3032 mounting a diamond wire of 0.3 mm diameter) into cubes with a surface of approximately 3x3 mm, which were then fixed on an AFM specimen holder with 2-4 mm clamping range by Leica. The small fragments of the sample were cut directly without embedding in resin. The sample holder was fixed on a flat XYZ scanning piezoelectric stage mounted on the ultramicrotome arm. The sectioning was performed by a vertical movement of the specimen over the extremely sharp blade of a fixed knife. Firstly, the surface of the sample was flattened by removal of several (1 µm thick) layers with a triangular tungsten carbide knife (Electron Microscopy Sciences, 40° cutting angle) adjusted at 10° clearance angle to the sample surface.

Finally, thinner sections (500, 200 and 100 nm layers) were trimmed off the surface with a diamond knife (Diatome Histo, 45° cutting angle) adjusted at 6° clearance angle to the sample surface. The prepared surface from ultramicrotome was used for AFM measurement without any further surface treatment.

2.8. AFM measurements and data analysis - A Dimension ICON-2 FastScan Bio Atomic Force Microscope (Bruker Nano, Santa Barbara, CA, USA) was operated in the Force Volume mode to conduct single-molecule force spectroscopy (SMFS) with ScanAsyst powerful AFM control associated to Nanoscope V controller. The AFM was equipped with a FastScan Head 35 μm scan range system with temporal resolution of up to 3 frames-per-second for live sample observations using FastScan probe models. Triangular oxide sharpened silicon cantilevers of nominal spring constants of 0.25-0.45 N/ m (ScanAsyst-Air probes, Bruker Nano) were used for single-molecule force spectroscopy. Measuring the resonant frequency and the quality factor of the cantilever in air by the AFM thermal method allowed us to get the spring constant of the cantilever to standardize our AFM force measurements. In single-molecule force spectroscopy (SMFS) experiments, the AFM tip is continuously approached to and retracted from the biological sample, while monitoring the interaction force. The obtained force-extension curves provide key insight into the molecular elasticity and localization of single molecules, either on isolated systems or on cellular surfaces. The cantilever sensitivity was estimated from 50 forces curves, at least, on fused silica calibrate sample ($E_{modulus}$ = 72.9 GPa for cantilever spring constant K < 10 N/m) prior SMFS experiments. Overview images (25 × 25 μm^2) were recorded at imaging forces of 150 pN, the AFM tip was oscillated vertically at 8 kHz applying a 15 nm amplitude, the sample was scanned using a line frequency of 10 Hz, and 512 pixels were scanned per line (512 lines). Best high-resolution AFM topographs and interaction maps were found at imaging forces ≥150 pN, oscillation frequency ≤8 kHz, oscillation amplitudes between 10 and 30 nm, and line scanning frequencies ≤2.5 Hz. All FD-based AFM images were recorded in standard PBS buffer. For each SMFS experiment, a 250 nm ramp size and an interaction time from 0.1 to 10 s were used. We varied the loading rate from 10 nm/s to 1740 nm/s on a series of different transversal junctions, for selecting the optimal value for the loading rate. Identical scan rates were selected for the "extend and retract" motion of the functionalized probe. We also selected a contact point duration of 100 ms for all experiments. The control measurement was performed, by recording the adhesion maps from a non-functionalized tip in the same area than that scanned with the functionalized tip. Alternately, tips functionalized with biofunctionalized estrogen receptor probes were used as negative controls [53] to scan the surface of *Pinna nobilis* prismatic layer. No specific interactions were noticed, particularly along the periprismatic membranes. All experiments were performed in a temperature-controlled environment (25 °C).

2.9. Statistical analysis

At least thirty areas were scanned per sample type. The adhesion force distribution for a loading rate of 500 nm/s was quantified in the two sections (transversal, longitudinal) by performing statistics over 128x128 points per area; the data (average, standard deviation) were treated with Excel and a histogram was generated.

3. Results

3.1. Polyclonal antibodies against accripin11 – A polyclonal antibody was obtained against two accripin11 peptides. This unpurified antibody preparation represents a mix of immunoglobulins that target specifically each of the designed peptides of accripin11, according to the double X option immunization program developed by Eurogentec. In a first step, the antibody preparation was tested unpurified, *i.e.*, in the whole serum form, against the unfractionated acetic acid soluble prism matrix, which electrophoretic migration pattern is shown in Fig. 4A, lane 2, on the silver-stained gel. This matrix contained several discrete and non-discrete bands. When this matrix was blotted on a nitrocellulose membrane and tested by Western blot with the unpurified anti-accripin11 antibody preparation, the results revealed a single reactive band, as shown in Figure 4a, lane 4. Given the apparent molecular weight of the band, this corresponds to accripin11. This clearly demonstrated that the antibody preparation was accripin-specific and did not cross-react with other macromolecules of the prism matrix. This conclusive prerequisite step allowed us to go to the next step.

In a second step, the antibody was purified from its serum and the five eluted fractions obtained by affinity chromatography were partly denatured and tested on silver-stained gel (Figure 4b) and Western blot (Figure 4c). As shown by these two figures, antibody preparations on gel are characterized by three bands on a gel: one of very high molecular weight, corresponding to the full-size immunoglobulin molecule (IgG, between 130 and 170 kDa); the second intermediate band corresponds to the IgG heavy chain between 43 and 55 kDa, while the third lower band corresponds to the IgG light chain, slightly above 34 kDa. These results are in conformity with earlier finding on IgGs on SDS-PAGE gels [54]. The result of the simplified Western blot (single incubation with the secondary antibody, Figure 4c) confirms the identity of these three bands, as they all hybridize with the secondary goat-anti-rabbit antibody (GAR/AP). According to Figure 4b, eluates 3 and 4 (respectively, lanes 4 and 5) contain most of the purified antibody while eluates 2 and 5 (respectively lanes 3 and 6) contain traces, and eluate 1 (lane 2) is devoid of IgG. We pooled together the content of eluates 2 to 5 (lanes 3 to 6), to maximize the amount of usable antibody, before desalting the pooled eluates by dialysis against ultrapure water, followed by a spin concentration.

3.2. Mapping of the biomineral surface - Prior to biomineral surface scanning, we performed series of tests with loading rates varying from 10 nm/s to 1740 nm/s on a series of different periprismatic membranes, as shown by the graph of Figure 5. We obtained an increasing exponential curve. We selected 500 nm/s (2.7 in logarithmic scale) as the reference for the loading rate for the reported experiments. This represents a good compromise between acquisition speed and the risk of erosion of the functionalized tips. One has to consider that the interaction values are relative and depend on the acquisition speed, on the "extend and retract" motion of the probe, and on the contact duration between the functionalized probe and the specimen.

The results of the mapping experiments with functionalized tips acquired from prismatic layer samples prepared via ultramicrotomy are illustrated in Figures 6, 7 and 8. Figure 6 shows successively the 3D (Figure 6 a, d), 2D (Figures 6b, e) images and line profiles (Figures 6c, f) of the preparations, in transverse (Figure 6a-c) and longitudinal (Figure 6d-f) sections, respectively. In both sections, the periprismatic sheath appears slightly in relief, particularly in transverse section (Figure 6a). The mineral surface is not completely flat or uniform but exhibits a certain nano-rugosity and nano-porosity. However, all things considered, the differences of heights are minimal between the peri-prismatic sheath and the calcite surface as shown by the two profiles of figures 6c and 6f: at maximum, a difference of 160 nm is recorded in transverse section (Figure 6c) and 130 nm for figure 6c (longitudinal). The AFM tip can easily accommodate such height differences. Our multiple attempts showed that the ultramicrotomy procedure generates flatter surfaces than the mirror polishing followed by surface cleaning (see supplementary Figure 1c and d). We consider that a low height difference (below 200 nm) guarantees the quality of the results by excluding artifact signals such as non-specific adhesion due to topography.

Figure 7 presents adhesion maps with unfunctionalized tip (Figure 7a and c, negative control) and with the same tip that was functionalized with anti-accripin11 antibody (Figure 7b and d). The views represent transversal (Figures 7a and b) and longitudinal (Figure 7c and d) sections of the prisms. The adhesion forces varied between 0 to 2 nanonewtons in transverse section (Fig. 7b) this latter relative value corresponding to the antigen-antibody binding force. Therefore, white pixels in the adhesion maps shown in Figure 7b represent spots where the antigen-antibody binding-induced adhesion is recorded, in other words, where accripin11 is present. The control experiments (with unfunctionalized tips) show very few unspecific adhesion spots in transverse section (Figure 7a). For some unknown reasons, we recorded a higher background in the negative control of longitudinal sections (Figure 7c). However, one notices that a high density of white spots is observed on Figure 7d. In both ‘positive’ surfaces, on the mineral surface excluding the periprismatic sheath, accripin11 seems to be homogeneously distributed everywhere, without drawing any particular adhesion pattern. Prior to force spectroscopy measurements, topography in Peak Force QNM mode showed a high density of skeletal proteins along the ridges, typically about 100 to 150 proteins/µm. In addition, where the periprismatic sheaths are located, we observe a denser pattern of accripin11, suggesting that this protein is more concentrated at that particular site than on the mineral surface, *i.e.*, at the interface between the mineral itself and the periprismatic sheath. However, it is not clear whether the alignment of accripin11 along the sheaths is homogeneous or whether it may exhibit some variations. In Figure 7b, the sheath is hardly underlined, and the locations where the density of white spots is the highest are triple junctions of the sheath while, in Figure 7d, the sheath that crosses the picture from left to right is intensely marked.

Interestingly, in our attempt to quantify the interaction between the functionalized tip and the prism surface, we found out that in transverse section (perpendicular to the elongation axis of the prisms), the adhesion force is about twice higher (56 pN +/- 30pN) than in longitudinal sections (26 pN +/- 17 pN) parallel to the elongation axis, as shown by the histogram of Figure 8. A possible reason of this difference is discussed below. We have not considered multiples of the single average force. This is because our probe can, in some areas, probe two or three proteins at the contact point. Its multiple interactions have been documented in previous publication [36]. As negative control, as expected, negligible adhesion forces were recorded for spots with no accripin11, in both sections.

4. Discussion

In this paper, we describe a novel methodology to localize biomineralization proteins on the surface of biominerals. To our knowledge, this is the first time that this technique is applied in the field of biomineralization. Until recently, there have been a number of attempts to visualize the distribution of organics throughout a biomineral, but each of them has significant limitations: Muyzer and Westbroek [55] used immunohistological techniques to visualize bulk organic matrix in shells via optical microscopy. Their approach based on mixtures of macromolecules for eliciting the polyclonal antibody lacked specificity and resolution. These two pitfalls were partly overcome (1) by raising more specific antibodies against single shell proteins, and (2) by using gold-coupled secondary antibodies to amplify the signals and allow SEM observations in back-scattered electron mode [56, 57]. The technique was pushed to its limits by double labelling for a target protein and chitin [58]. While the immunogold approach undoubtedly represents a milestone, it is limited to intermediate magnifications, typically between 1,000x to 20,000x, and requires most of the time a final silver enhancement step to increase the signal by precipitating silver around the gold nanoparticles. However, this step can induce false positive signals if the shell contains traces of heavy metals that can also react with silver [59]. Another drawback is that the surface of the sample, covered by blocking agent (BSA, gelatin or carbohydrate-free reagent), antibodies, gold and silver particles, cannot be reused for other purposes, like EDX or WDS investigations. Histochemical staining is another method used [60] to map reactive chemical groups on the surface of nacre tablets. However the technique does not give structural information on the macromolecules that carry the reactive groups. Atom probe tomography has been applied at the nanoscale [61], but here again, the interacting organic molecules cannot be identified. Finally, mapping by micro- or nano-FTIR or Raman spectrometry are useful, but these techniques are limited to chemical reactive groups [62, 63] or pigments [64]. In addition, in spite of reaching the 'nano' level, they lack the lateral resolution required for precise localization of the reactive groups. The AFM approach that we use here overcomes many of these limitations. In particular, it can answer the question of affinity of the protein of interest with the mineral phase. This in turn has a direct implication on which non-classical crystallization pathway is selected for building the studied biomineral. For example, 'inter-crystalline' proteins (*i.e.*, proteins that constitute the sheath 'surrounding' a given crystal unit) tend to exhibit hydrophobic properties due to their enrichment in aliphatic amino acids. At the scale of a single crystal (micrometric to sub-micrometric scale), the location of such proteins is governed by a 'segregation mechanism' (*i.e.*, a phase separation) from the aqueous mineral front, which grows from a center and progresses radially. Consequently, these proteins condense (by cross-linking) into a soft and flexible but water-insoluble barrier surrounding the crystal, as soon as this latter enters into confluence with its immediate neighbor crystals. In contrast, 'intracrystalline' proteins, which are more hydrophilic, stay disseminated, at the nanoscale, in the vicinity of the nascent (usually amorphous) nanograins that will become welded to their neighbor nanograins according to a nanoscale assembly process [65]. The nanograin welding leads to the trapping of these hydrophilic proteins, which can consequently be considered as truly occluded (‘intracrystalline’) in the forming crystal.

In the present case, we obtained mapping of accripin11 at the surface of the calcitic prisms of *Pinna nobilis,* in two sections perpendicular to each other, the transverse section and the longitudinal ones. For each of these surfaces, we obtained an even distribution of accripin11, implying that this protein should be considered primarily as intracrystalline. Moreover, we observed that accripin11 was slightly more concentrated along the periprismatic sheaths, suggesting that it may be intercrystalline as well. A possible explanation of this duality might originate from the amphiphilic nature of accripin11 sequence, with a hydrophobic N-terminus and a hydrophilic C-terminus. In our scanning experiments, we noticed that the adhesion force in transverse section was twice as high than that of longitudinal section. This finding is particularly interesting because it means that the accessibility of the antibodies to the target accripin 11 differs, depending on the orientation of the section: in other words, the antigen-antibody recognition seems to be hindered in longitudinal sections in comparison to transverse sections. This decrease of recognition may have something to do with the very close environment of the complex, including both the mineral phase and other surrounding matrix macromolecules. Going further, if accripin11 was randomly oriented on the surface, there should be no statistical difference between the longitudinal and transversal sections. But since the adhesion forces are significantly different, this suggests obviously that accripin11 is not randomly oriented at the surface of the prism section, but has probably preferential orientations in the biomineral. This is the most likely explanation of the adhesion difference between the two sections. At this stage, our assertion is speculative, but if supported by other approaches such as solid-state Nuclear Magnetic Resonance (ss-NMR) and structure prediction [66], we have an elegant – although indirect - manner to detect preferential orientations of some matrix macromolecules in biominerals.

In order to be utilized optimally, Single Molecule Force Spectroscopy (SMFS) has some specific requirements: a highly purified and specific antibody, an efficient functionalization of the AFM tip and an appropriate mineral surface preparation. The antibody must be pure and should recognize only one target-protein in a mixture of proteins. It is well known that antibodies that are supposedly specific of one given antigenic determinant can give unexpected cross-reactivity [67] or can cross-react with other proteins that exhibit similar determinants as the target protein [68, 69]. The gold-standard way to check antibody specificity is via Western blot and we highly recommend performing this prerequisite check in order to simplify the interpretation of AFM scans. In addition to antibody specificity, purifying the antibody from its serum is a mandatory step to get rid of all contaminating serum proteins (serum albumin, fibrinogen, transferrin, fetuin, lipoproteins). This step can be achieved in few hours with a kit. At last, purified antibody preparations contain salts that come from the eluent in addition to ionic components of the neutralizing buffer. These components can impair subsequent AFM tip functionalization steps. Therefore, before use in AFM experiments, we recommend dialysis of the purified antibody solution, to remove these salts, followed by concentration of the antibody in a centrifugal concentrator tube.

Functionalization of the AFM tip is another critical step. The antibody must be covalently bound, for maintaining a stronger bond to the tip than between the antibody and its target antigen. We adopted an extremely simple tip functionalization procedure [50, 52], which required a limited number of steps and reactants. In our hands, this maximized the rate of success. As the functionalization was made 'blind', its effectiveness was checked *a posteriori* by performing the positive control experiment with the functionalized tip. We recommend preceding this positive control by a negative control performed with the same unfunctionalized tip, in the same area of the sample. At last, we also recommend preparing always fresh solutions for functionalization: attempts made with old solutions led to complete failure of the experiment.

The third key element of our approach concerns sample preparation. In conventional AFM mapping, samples are prepared by mirror polishing. Over several pilot trials, we found that preparation of the surface by ultramicrotomy provided more consistent results than by mirror polishing, mainly because of the lower roughness (around 100-150 nm) and the absence of any surface treatment (see supplementary figure 1). Although the polishing/cleaning approach could be optimized with 30 nm colloidal silica, the post-polishing treatment - including desorption with a surfactant like Tween20 to remove surface contaminants, ‘bleaching’ with dilute sodium hypochlorite to clean the surface or slight etching (1 min.)

with dilute EDTA (1% w/vol) to expose occluded proteins - induced higher topography (EDTA treatment) and/or swelling of the periprismatic sheaths due to the Tween20 desorption step. So far, ultramicrotomy without any further treatment appears to be the optimal way to prepare biominerals surfaces for mapping of organics with functionalized AFM tips.

Despite the good resolution we achieved in mapping accripin11 across the surfaces of these calcitic prisms, our approach is not without its limitations. Using glutaraldehyde to functionalize the AFM tip poses a challenge in controlling the density of proteins on the tip surface. Furthermore, antibody attachment to the tip is achieved randomly, *i.e.*, the antigen binding sites of the antibody are not all optimally oriented for surface scanning. Thus, only a part of the antibody-occupied sites on the AFM tip will be correctly oriented to interact with their corresponding target antigen [50]. As underlined before, the functionalization is made 'blind' and is empirically optimized; its effectiveness is assessed *a posteriori* during data acquisition. The tip, once functionalized, is also not stable. A functionalized AFM tip can only last a maximum of 3 days in PBS buffer at 4 °C [52], with the best scanning results achieved directly after functionalization of the tip. Specific and non-specific interactions between the tip and the surface can also be difficult to distinguish. The use of a spacer, like PEG, may partly solve this problem, however tip functionalization becomes more complicated and tedious to implement with these additional steps [36, 70]. As we emphasize above, surface preparation is critical, and if target antigens are not firmly bound to the sample surface, then they can adhere to the tip during data acquisition and thereby pollute it. The end result is an inactivated tip. Finally, surface preparation requires an ultramicrotome for hard tissues, a sophisticated and costly device.

In spite of these limitations, we assert that the technique brings substantial improvements to alternative approaches. For instance, the resolution of the technique is higher than that of immuno-labelling approaches; proteins can be localized at the nanometer scale and does not require any labels to be fixed to the biomineral surface. As a consequence, scanning a surface with a functionalized tip leaves the mineral surface clean in contrast to immunogold staining, and so the surface can be re-used for other physical investigations such as EDX, WDS, FTIR or Raman spectroscopies. These characterizations are not possible after immunogold staining. Tip functionalization also allows for the estimation of antigen-antibody interactions with piconewton accuracy. When performed via the glutaraldehyde pathway, the process is quite simple and does not require complex chemical modification of the tip. The procedure is rather rapid (2 hours), which means that the functionalization of few tips can be tested in a day. An efficient way of operating consists in performing a set of negative controls with different unfunctionalized tips, and to start the functionalization of the first tip during while the second and following tips are tested in negative controls. Finally, the use of ultramicrotome to prepare the flat sample surfaces for measurement eliminates the chances of spreading protein or contamination and thus, eliminates the requirement of surface treatment that may induce artifacts by increasing surface topography.

To conclude, the technique, as exposed here, is adapted to skeletal proteins, the most abundant macromolecules identified in calcium carbonate biominerals. While our study employs a mollusc shell and may appear to be fringe case, we are confident that our approach has a general scope and is adaptable to many types of biominerals including calcium phosphate (bone, teeth), calcium oxalates, silica, or any type of biomineral, resulting from a biologically-controlled or biologically-induced deposition process. In particular, pathological biomineralizations such as kidney or pancreatic stones may benefit from this advancement: because they contain a complex cortege of proteins [71, 72], localizing precisely the most abundant ones may help elucidating the molecular mechanism by which these minerals form, with a resolution far beyond what is currently done. The technique can also be applied to calcium phosphate-coated bone / teeth implants where the coating is doped or co-precipitated with one or more bioactive macromolecules, such as growth factors (BMPs) or peptides/proteins that enhance cellular attachment to improve osseointegration [73, 74]. We assert that the technique may precisely quantify the density of protein per square unit, in other words, evaluate the rate of protein incorporation in the coating. In clinical tests using similar samples in terms of preparation, the acquisition could be automated to allow analyzing ten samples a day with 3 analyzed areas per sample, on the assumption that the AFM probe is qualified once. At the end of the series, the first sample should be re-analyzed in order to confirm the successive analyses. Because of its sensitivity, the technique can also be applied in archeology or paleobiology, on fossil or subfossil shell or bone materials that contain only remains of mineralizing matrix [75]. At last, in addition to proteins, AFM mapping with functionalized tips can localize other types of macromolecules, such as polysaccharides, the second most abundant components of skeletal matrices. In that case, antibodies may usefully be replaced by specific lectins. To summarize, we believe that this technique will bring valuable information in terms of functions of organics in biomineralization process.

Acknowledgments

The study has been financially supported by ANR MOBi (ANR-18-CE02-0014-02, 2018-2023, J. Perrin, coordinator), including the salary of B. Kurshid and most of the consumables and chemicals. Other financial supports include 1) the Research Project of Excellence BFC "PIA-Récolnat-BFC" supported by region Burgundy - Franche-Comté and the "Récolnat ANR-11-INBS-0004" program (JT), 2) two SRO projects, one in 2017, one in 2020 ('Pinocchio', PInna NObilis & sa Calcification Coquillière: une Histoire Originale) attributed to FM by OSU-Theta (Bourgogne - Franche-Comté), 3) a grant from EMBRC (European Marine Biological Resource Centre, FM), which provided the logistic support for a field mission to collect living specimens of *Pinna nobilis* at Villefranche-sur-Mer marine station in spring 2017. All the authors greatly acknowledge the DDTM of Alpes Maritimes (Julien Banus, Serge Castel) for having issued the authorization (Arrêté Préfectoral n° 2017-459) to sample *Pinna nobilis*.

Author contribution

Benazir Khurshid: formal analysis, investigation, methodology, validation, visualization, writing - original draft preparation, review and editing. Eric Lesniewska: investigation, methodology, resources, visualization. Luca Polacchi: resources, writing - original draft. Maëva L’Héronde: resources. Daniel J. Jackson: writing – original draft, review and editing. Sebastien Motreuil: resources. Jérôme Thomas:

visualization, funding acquisition. Jean-François Bardeau: conceptualization, formal analysis, writing – original draft. Stephan E. Wolf: conceptualization, writing – original draft. Daniel Vielzeuf: conceptualization, funding acquisition. Jonathan Perrin: conceptualization, funding acquisition. Frédéric Marin: conceptualization, data curation, formal analysis, investigations, methodology, project administration, resources, supervision, validation, visualization, writing – original draft, review and editing.

The authors have no conflict of interest.

References:

[1] B. Khurshid, D.J. Jackson, S. Engilberge, S. Motreuil, C. Broussard, J. Thomas, F. Immel, M.J. Harrington, P.B. Crowley, D. Vielzeuf, J. Perrin, F. Marin, Molecular characterization of accripin11, a soluble shell protein with an acidic C-terminus, identified in the prismatic layer of the Mediterranean fan mussel Pinna nobilis (Bivalvia, Pteriomorphia), FEBS Open Bio 13 (2023) 10-25.

[2] H.A. Lowenstam, S. Weiner, On biomineralization, Oxford University Press New York, 1989.

[3] A. Knoll, Biomineralization and Evolutionary History, Reviews in Mineralogy & Geochemistry 54 (2003) 329-356.

[4] J. Aizenberg, A. Tkachenko, S. Weiner, L. Addadi, G. Hendler, Calcitic microlenses as part of the photoreceptor system in brittlestars, Nature 412 (2001) 819-822.

[5] W. Dong, H. Cheng, Y. Yao, Y. Zhou, G. Tong, D. Yan, Y. Lai, W. Li, Bioinspired synthesis of calcium carbonate hollow spheres with a nacre-type laminated microstructure, Langmuir 27 (2011) 366-370.

[6] K. Lee, W. Wagermaier, A. Masic, K.P. Kommareddy, M. Bennet, I. Manjubala, S.-W. Lee, S.B. Park, H. Cölfen, P. Fratzl, Self-assembly of amorphous calcium carbonate microlens arrays, Nature Communications 3 (2012) 725.

[7] M. Różycka, I. Coronado, K. Brach, J. Olesiak-Bańska, M. Samoć, M. Zarębski, J. Dobrucki, M. Ptak, E. Weber, I. Polishchuk, B. Pokroy, J. Stolarski, A. Ożyhar, Lattice shrinkage by incorporation of recombinant starmaker-like protein within bioinspired calcium carbonate crystals, Chemistry – A European Journal 25 (2019) 12740-12750.

[8] A. Jackson, J. Vincent, R.M. Turner, The Mechanical Design of Nacre, Proceedings of The Royal Society of London 234 (1988) 415-440.

[9] J.G. Carter, Skeletal Biomineralization: Patterns, Processes and Evolutionary Trends, Van Nostrand Reinhold, New York, 1990.

[10] J.-P. Cuif, Y. Dauphin, A. Denis, D. Gaspard, J. Keller, Etude des caracteristiques de la phase minerale dans les structures prismatiques du tests de quelques Mollusques, Bulletin du Muséum National d'Histoire Naturelle de Paris 4e sér. sect. A (1983) 679-717.

[11] W.J. Schmidt, Die Bausteine des Tierkörpers in polarisiertem Lichte, F. Cohen, Bonn, Germany, 1924.

[12] H. Cölfen, M. Antonietti, Mesocrystals: inorganic superstructures made by highly parallel crystallization and controlled alignment, Angewandte Chemie International Edition 44 (2005) 5576-5591.

[13] H. Cölfen, M. Antonietti, Mesocrystals and Nonclassical Crystallization, John Wiley & Sons, Ltd., Chichester, 2008.

[14] J.J. De Yoreo, P.U.P.A. Gilbert, N.A.J.M. Sommerdijk, R.L. Penn, S. Whitelam, D. Joester, H. Zhang, J.D. Rimer, A. Navrotsky, J.F. Banfield, A.F. Wallace, F.M. Michel, F.C. Meldrum, H. Cölfen, P.M. Dove, Crystallization by particle attachment in synthetic, biogenic, and geologic environments, Science 349 (2015) aaa6760.

[15] S.E. Wolf, C.F. Böhm, J. Harris, B. Demmert, D.E. Jacob, M. Mondeshki, E. Ruiz-Agudo, C. Rodríguez-Navarro, Nonclassical crystallization in vivo et in vitro (I): Process-structure-property relationships of nanogranular biominerals, Journal of Structural Biology 196 (2016) 244-259.

[16] C. Rodríguez-Navarro, E. Ruiz-Agudo, J. Harris, S.E. Wolf, Nonclassical crystallization in vivo et in vitro (II): Nanogranular features in biomimetic minerals disclose a general colloid-mediated crystal growth mechanism, Journal of Structural Biology 196 (2016) 260-287.

[17] F. Marin, N. Le Roy, B. Marie, The formation and mineralization of mollusk shell, Frontiers in Bioscience (Scholar edition) 4 (2012) 1099-1125.

[18] I. Weiss, V. Schönitzer, N. Eichner, M. Sumper, The chitin synthase involved in marine bivalve mollusk shell formation contains a myosin domain, FEBS Letters 580 (2006) 1846-1852.

[19] I. Herlitze, B. Marie, F. Marin, D.J. Jackson, Molecular modularity and asymmetry of the molluscan mantle revealed by a gene expression atlas, GigaScience 7 (2018) giy056.

[20] F. Marin, B. Marie, S. Hamada, P. Ramos-Silva, N. Le Roy, N. Guichard, S. Wolf, C. Montagnani, C. Joubert, D. Piquemal, D. Saulnier, Y. Gueguen, 'Shellome': Proteins Involved in Mollusc Shell Biomineralization —Diversity, Functions., in: S. Watabe, K. Maeyama, H. Nagasawa (Eds.), Recent Advances in Pearl Research - Proceedings of the International Symposium on Pearl Research 2011, Terrapub, Tokyo, 2013, pp. 149-166.

[21] F. Marin, Mollusc shellomes: Past, present and future, Journal of Structural Biology 212 (2020) 107583.

[22] T. Yarra, M. Blaxter, M.S. Clark, A Bivalve Biomineralization Toolbox, Molecular Biology and Evolution 38 (2021) 4043-4055.

[23] S. Cohen, E. Kalfon-Cohen, Dynamic nanoindentation by instrumented nanoindentation and force microscopy: A comparative review, Beilstein Journal of Nanotechnology 4 (2013) 815-833.

[24] U. Dammer, M. Hegner, D. Anselmetti, P. Wagner, M. Dreier, W. Huber, H.J. Güntherodt, Specific antigen/antibody interactions measured by force microscopy, Biophysical Journal 70 (1996) 2437-2441.

[25] P.K. Hansma, J.P. Cleveland, M. Radmacher, D.A. Walters, P.E. Hillner, M. Bezanilla, M. Fritz, D. Vie, H.G. Hansma, C.B. Prater, J. Massie, L. Fukunaga, J. Gurley, V. Elings, Tapping mode atomic force microscopy in liquids, Applied Physics Letters 64 (1994) 1738-1740.

[26] M. Pfreundschuh, D. Alsteens, M. Hilbert, M.O. Steinmetz, D.J. Müller, Localizing Chemical Groups while Imaging Single Native Proteins by High-Resolution Atomic Force Microscopy, Nano Letters 14 (2014) 2957-2964.

[27] M. Rief, M. Gautel, F. Oesterhelt, J.M. Fernandez, H.E. Gaub, Reversible unfolding of individual titin immunoglobulin domains by AFM, Science 276 (1997) 1109-1112.

[28] C.S. Sikes, A. Wierzbicki, V.J. Fabry, From atomic to global scales in biomineralization, Bulletin de l'Institut Océanographique 14 (1994) 1-47.

[29] S. Manne, C.M. Zaremba, R. Giles, L. Huggins, D.A. Walters, A. Belcher, D.E. Morse, G.D. Stucky, J.M. Didymus, S. Mann, P.K. Hansma, Atomic force microscopy of the nacreous layer in mollusc shells, Proceedings of the Royal Society of London. Series B: Biological Sciences 256 (1994) 17-23.

[30] A.G. Checa, C.M. Pina, A.J. Osuna-Mascaró, A.B. Rodríguez-Navarro, E.M. Harper, Crystalline organization of the fibrous prismatic calcitic layer of the Mediterranean mussel *Mytilus galloprovincialis*, European Journal of Mineralogy 26 (2014) 495-505.

[31] S. Senapati, S. Lindsay, Recent progress in molecular recognition imaging using Atomic Force Microscopy, Accounts of Chemical Research 49 (2016) 503-510.

[32] H. Clausen-Schaumann, M. Seitz, R. Krautbauer, H.E. Gaub, Force spectroscopy with single bio-molecules, Current Opinion in Chemical Biology 4 (2000) 524-530.

[33] T.E. Fisher, P.E. Marszalek, J.M. Fernandez, Stretching single molecules into novel conformations using the atomic force microscope, Nature Structural Biology 7 (2000) 719-724.

[34] C.D. Frisbie, L.F. Rozsnyai, A. Noy, M.S. Wrighton, C.M. Lieber, Functional Group Imaging by Chemical Force Microscopy, Science 265 (1994) 2071-2074.

[35] S. Allen, J. Davies, M.C. Davies, A.C. Dawkes, C.J. Roberts, S.J.B. Tendler, P.M. Williams, The influence of epitope availability on atomic-force microscope studies of antigen–antibody interactions, Biochemical Journal 341 (1999) 173-178.

[36] P. Hinterdorfer, W. Baumgartner, H. Gruber, K. Schilcher, H. Schindler, Detection and localization of individual antibody-antigen recognition events by Atomic Force Microscopy, Proceedings of the National Academy of Sciences of the United States of America 93 (1996) 3477-3481.

[37] Y. Jiang, C. Zhu, L. Ling, L. Wan, X. Fang, C. Bai, Specific Aptamer−Protein Interaction Studied by Atomic Force Microscopy, Analytical Chemistry 75 (2003) 2112-2116.

[38] J.S. Kim, S. Jang, U. Kim, K. Cho, AFM Studies of Inhibition Effect in Binding of Antimicrobial Peptide and Immune Proteins, Langmuir 23 (2007) 10438-10440.

[39] H. Wang, Y. Dalal, S. Henikoff, S. Lindsay, Single-epitope recognition imaging of native chromatin, Epigenetics & Chromatin 1 (2008) 1-9.

[40] P.-H. Puech, K. Poole, D. Knebel, D.J. Muller, A new technical approach to quantify cell–cell adhesion forces by AFM, Ultramicroscopy 106 (2006) 637-644.

[41] A.V. Taubenberger, D.W. Hutmacher, D.J. Muller, Single-Cell Force Spectroscopy, an Emerging Tool to Quantify Cell Adhesion to Biomaterials, Tissue Engineering Part B: Reviews 20 (2013) 40-55.

[42] V.T. Moy, E.L. Florin, H.E. Gaub, Intermolecular forces and energies between ligands and receptors, Science 266 (1994) 257-259.

[43] B. Marie, G. Luquet, J.-P. Pais De Barros, N. Guichard, S. Morel, G. Alcaraz, L. Bollache, F. Marin, The shell matrix of the freshwater mussel *Unio pictorum* (Paleoheterodonta, Unionoida). Involvement of acidic polysaccharides from glycoproteins in nacre mineralization., The FEBS Journal 274 (2007) 2933-2945.

[44] J.H. Morrissey, Silver stain for proteins in polyacrylamide gels: A modified procedure with enhanced uniform sensitivity, Analytical Biochemistry 117 (1981) 307-310.

[45] P. Matsudaira, Sequence from picomole quantities of proteins electroblotted onto polyvinylidene difluoride membranes, Journal of Biological Chemistry 262 (1987) 10035-10038.

[46] S. Allen, X. Chen, J. Davies, M.C. Davies, A.C. Dawkes, J.C. Edwards, C.J. Roberts, J. Sefton, S.J.B. Tendler, P.M. Williams, Detection of antigen−antibody binding events with the Atomic Force Microscope, Biochemistry 36 (1997) 7457-7463.

[47] A. Vinckier, I. Heyvaert, A. D'Hoore, T. McKittrick, C. Van Haesendonck, Y. Engelborghs, L. Hellemans, Immobilizing and imaging microtubules by atomic force microscopy, Ultramicroscopy 57 (1995) 337-343.

[48] A. Yersin, H. Hirling, P. Steiner, S. Magnin, R. Regazzi, B. Hüni, P. Huguenot, P. De Los Rios, G. Dietler, S. Catsicas, S. Kasas, Interactions between synaptic vesicle fusion proteins explored by atomic force microscopy, Proceedings of the National Academy of Sciences of the United States of America 100 (2003) 8736-8741.

[49] G. Leclercq, I. Laïos, C. Elie-Caille, D. Leiber, G. Laurent, E. Lesniewska, Z. Tanfin, Y. Jacquot, ERα dimerization: a key factor for the weak estrogenic activity of an ERα modulator unable to compete with estradiol in binding assays, Journal of Receptors and Signal Transduction 37 (2017) 149-166.

[50] B. Alexandre, O. Ben, Common approaches to tip functionalization for AFM-based molecular recognition measurements, Bruker guide, Application Note #130 (2010).

[51] P. Silberzan, L. Leger, D. Ausserre, J.J. Benattar, Silanation of silica surfaces. A new method of constructing pure or mixed monolayers, Langmuir 7 (1991) 1647-1651.

[52] G. Lykotrafitis, AFM tip functionalization with glutaraldehyde, protocols.io (2019).

[53] Y. Jacquot, D. Spaggiari, J. Schappler, E. Lesniewska, S. Rudaz, and G. Leclercq, ERE-dependent transcription and cell proliferation: Independency of these two processes mediated by the introduction of a sulfone function into the weak estrogen estrothiazine, European Journal of Pharmaceutical Sciences 109 (2017) 169-181.

[54] V. Filipe, R. Poole, O. Oladunjoye, K. Braeckmans, W. Jiskoot, Detection and Characterization of Subvisible Aggregates of Monoclonal IgG in Serum, Pharmaceutical Research 29 (2012) 2202-2212.

[55] G. Muyzer, P. Westbroek, An immunohistochemical technique for the localization of preserved biopolymeric remains in fossils, Geochimica et Cosmochimica Acta 53 (1989) 1699-1702.

[56] F. Marin, P. Narayanappa, S. Motreuil, Acidic shell proteins of the Mediterranean fan mussel Pinna nobilis, in: W.E.G. Müller (Ed.), Molecular Biomineralization: Aquatic Organisms Forming Extraordinary Materials, Springer Berlin Heidelberg, Berlin, Heidelberg, 2011, pp. 353-395.

[57] F. Marin, B. Pokroy, G. Luquet, P. Layrolle, K. De Groot, Protein mapping of calcium carbonate biominerals by immunogold, Biomaterials 28 (2007) 2368-2377.

[58] A.J. Osuna-Mascaró, T. Cruz-Bustos, F. Marin, A.G. Checa, Ultrastructure of the interlamellar membranes of the nacre of the bivalve Pteria hirundo, determined by immunolabelling, PLOS ONE 10 (2015) e0122934.

[59] A. Osuna-Mascaró, T. Cruz Bustos, B. Marie, A. Checa, F. Marin, Heavy Metals in Mollusc Shells: A Quick Method for their Detection, Key Engineering Materials 672 (2015) 340-346.

[60] F. Nudelman, B. Gotliv, L. Addadi, S. Weiner, Mollusk shell formation: Mapping the distribution of organic matrix components underlying a single aragonitic tablet in nacre, Journal of Structural biology 153 (2006) 176-187.

[61] L.M. Gordon, D. Joester, Nanoscale chemical tomography of buried organic–inorganic interfaces in the chiton tooth, Nature 469 (2011) 194-197.

[62] S. Amarie, P. Zaslansky, Y. Kajihara, G. Erika, W. Schmahl, F. Keilmann, Nano-FTIR chemical mapping of minerals in biological materials, Beilstein Journal of Nanotechnology 3 (2012) 312-323.

[63] N. Trinkler, M. Labonne, F. Marin, A. Jolivet, M. Bohn, C. Poulain, J.F. Bardeau, C. Paillard, Clam shell repair from the brown ring disease: A study of the organic matrix using Confocal Raman micro-spectrometry and WDS microprobe, Analytical and Bioanalytical Chemistry 396 (2010) 555-567.

[64] C. Hedegaard, J.F. Bardeau, D. Chateigner, Molluscan shell pigments: an *in situ* Resonance Raman Study, Journal of Molluscan Studies 72 (2006) 157–162.

[65] R. Hovden, S.E. Wolf, M.E. Holtz, F. Marin, D.A. Muller, L.A. Estroff, Nanoscale assembly processes revealed in the nacroprismatic transition zone of Pinna nobilis mollusc shells, Nature Communications 6 (2015) 10097.

[66] D. L. Masica and J. J. Gray, Solution-and Adsorbed-State Structural Ensembles Predicted for the Statherin-Hydroxyapatite System, Biophysical Journal 96 (2009) 3082–3091.

[67] L. Faye, M.J. Chrispeels, Common antigenic determinants in the glycoproteins of plants, molluscs and insects, Glycoconjugate Journal 5 (1988) 245-256.

[68] V. Mouchi, F. Lartaud, N. Guichard, F. Immel, M. de Rafélis, C. Broussard, Q.G. Crowley, F. Marin, Chalky versus foliated: a discriminant immunogold labelling of shell microstructures in the edible oyster Crassostrea gigas, Marine Biology 163 (2016) 1-5.

[69] J.R. Rao, S.C. Yadav, G.C. Ram, P.R.S. Raghav, R.B. Lal, Common antigenic determinants of Fasciola gigantica as defined by monoclonal antibodies to phosphocholine, Journal of Applied Animal Research 9 (1996) 95-104.

[70] J.K. Stuart, V. Hlady, Effects of Discrete Protein-Surface Interactions in Scanning Force Microscopy Adhesion Force Measurements, Langmuir 11 (1995) 1368-1374.

[71] D.C. Zhang, J.B. Xiang, L.Y. Wang, Z.B. Xu, L.D. Sun, F. Zhou, X.L. Zha, D. Cai, Comparative Proteomic Analysis of Gallbladder Bile Proteins Related to Cholesterol Gallstones, PLOS ONE 8 (2013) art n° e54489.

[72] P. Peerapen, V. Thongboonkerd, Kidney stone proteomics: an update and perspectives, Expert Review of Proteomics 18 (2021) 557-569.

[73] Y. Liu, C. Schouten, O. Boerman, G. Wu, J.A. Jansen, E.B. Hunziker, The kinetics and mechanism of bone morphogenetic protein 2 release from calcium phosphate-based implant-coatings, Journal of Biomedical Materials Research Part A 106 (2018) 2363-2371.

[74] C.D. Reyes, T.A. Petrie, K.L. Burns, Z. Schwartz, A.J. García, Biomolecular surface coating to enhance orthopaedic tissue healing and integration, Biomaterials 28 (2007) 3228-3235.

[75] J. Sakalauskaite, F. Marin, B. Pergolizzi, B. Demarchi, Shell palaeoproteomics: first application of peptide mass fingerprinting for the rapid identification of mollusc shell in archaeology, Journal of Proteomics 227 (2020), 103920.

Figures captions

Figure 1. The shell of *Pinna nobilis.* a) Inner view of the right valve of an adult specimen. The internal nacreous layer (NL, whitish, delineated by a black dashed line) covers less than one half of the shell, contrarily to the prismatic outer layer (PL, brown-red). b) Inner SEM view of the prismatic layer, that consists of needles of polygonal section that are densely packed together and glued by thin interprismatic sheaths (dark line). The blue arrow symbolizes the growth axis of the prisms. c) An isolated single prism observed by SEM. Note that the prism is not homogeneous but constituted of a stack of thin mineralized layers perpendicular to its elongation axis.

Figure 2. (a) Amino acid sequence of accripin11, the protein of the prismatic layer, localized in this study by AFM with functionalized tip. The signal peptide is indicated in red. The two domains underlined in yellow and grey correspond to the two synthetic peptides used for generating polyclonal antibodies in white rabbits. (b) 3D-structure of accripin11, deduced from AlphaFold2 simulation. The two alpha helices are stabilized by four disulfide bonds while the C-terminus is disordered.

Figure 3. Principle of AFM surface scanning with functionalized tip. a) General scheme of molecular recognition imaging measurements in which ligand molecules (A) are attached to the AFM tip, whereas receptor molecules (B) are present on the sample surface. The tip is symbolized in grey. b) The amine group was introduced by silanization reaction between silicon surface of the tip and a trichlorosilane group of APTES, the silane reagent. After silanization, glutaraldehyde was used as a binding agent to attach antibodies (IgG) covalently to the tip. c) Typical Force-Distance curves recorded upon approach (blue curve) and retraction (red curve). The black triangles symbolize the AFM tip in different positions. From position 1–2, the tip is approaching the biomineral surface. Then, the cantilever bends until the force reaches the maximum limit as shown in position 3. The tip starts withdrawing at position 4 that further detaches from the surface and returns to its resting position 5. d)

more detailed theoretical view of the interaction between the antibody-grafted tip and the surface of the sample with the target protein.

Figure 4. Specificity of the anti-accripin11 antibody preparation. a) Test of the unpurified antibody against the soluble prims matrix. The soluble prism matrix, which contains several discrete bands, was checked on a monodimensional SDS-PAGE gel stained with silver (lane 2) and tested in parallel against the unpurified anti-accripin11 antibody (lane 4). Note the specificity of the antibody. Lanes 1 and 3: prestained molecular markers. b) Purification of the anti-accripin11 immunoglobulins after their elution from the affinity chromatography column. Lanes 2 to 6 correspond to eluates 1 to 5. Note that most of the immunoglobulins are concentrated in eluates 3 and 4 (lanes 4 and 5). Lane 1: molecular weight markers. c) Same gel as Fig. 4b electroblotted on a nitrocellulose membrane and directly tested against the secondary antibody (Goat anti-Rabbit, Alkaline Phosphatase conjugate). The three bands correspond, from top to bottom, to the full IgG, to the heavy chain and to the light chain, respectively.

Figure 5. Interaction force (pN) measured on *Pinna nobilis* periprismatic membranes for various loading rates from 10 to 1740 nm/s, expressed on a logarithmic scale. For all further experiments, a loading rate of 500 nm/s was selected.

Figure 6. AFM on the calcitic prisms of *Pinna nobilis*. Topographic images in transverse (a, b, c) and in longitudinal (d, e, f) sections, prepared by microtomy: a and d correspond to a 3D block of the surface topography of a prism, b and e, to a 2D image and c and f, to the topographic curve across the periprismatic sheath. In b and e, the white bar symbolizes the sections illustrated by c and f. Note that the difference of height is, at maximum (see c) 140 nm between the top of the periprismatic sheath and the mineral surface, and in general less than 100 nm (f). The AFM tip can accommodate such a difference.

Figure 7. AFM scanning of a prism surface, in transverse (a, b) and longitudinal (c, d) sections, adhesion maps. The surface was prepared by microtomy, without polishing. Figures a and c represent negative controls obtained with non-functionalized tips, while figures b and d are positive controls obtained with accripin11-functionalized tips. The numerous white dots correspond to locations where the adhesion between the functionalized tip and the surface is the highest, *i.e.*, where accripin11 is present. Accripin11 seems to be homogeneously distributed in the prism, but presents also high concentrations along the periprismatic sheaths in d, and at the triple junctions in b. For each of the four maps, the scales are relative.

Figure 8. Interaction force measured on *Pinna nobilis* transversal and longitudinal sections, for a loading rate of 500 nm/s. The two negative control histograms (A and C) correspond to zones devoid of accripin11. Note the difference in adhesion in transversal (B) and longitudinal (D) sections.

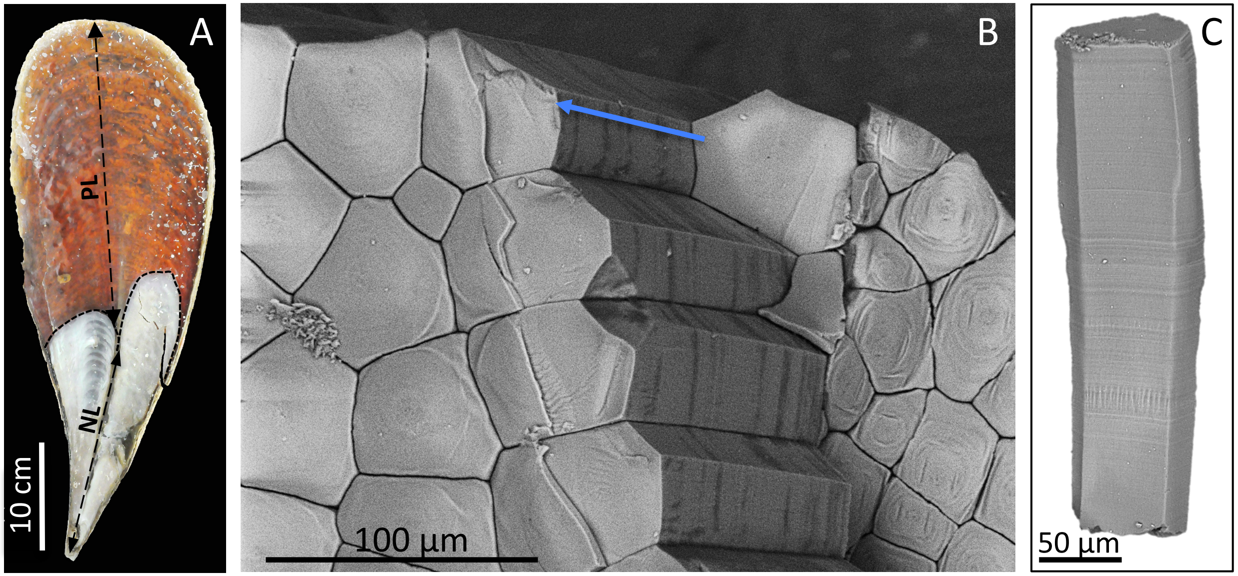
A
PL
NL
10 cm
B
100 µm
C
50 µm

Figure 2

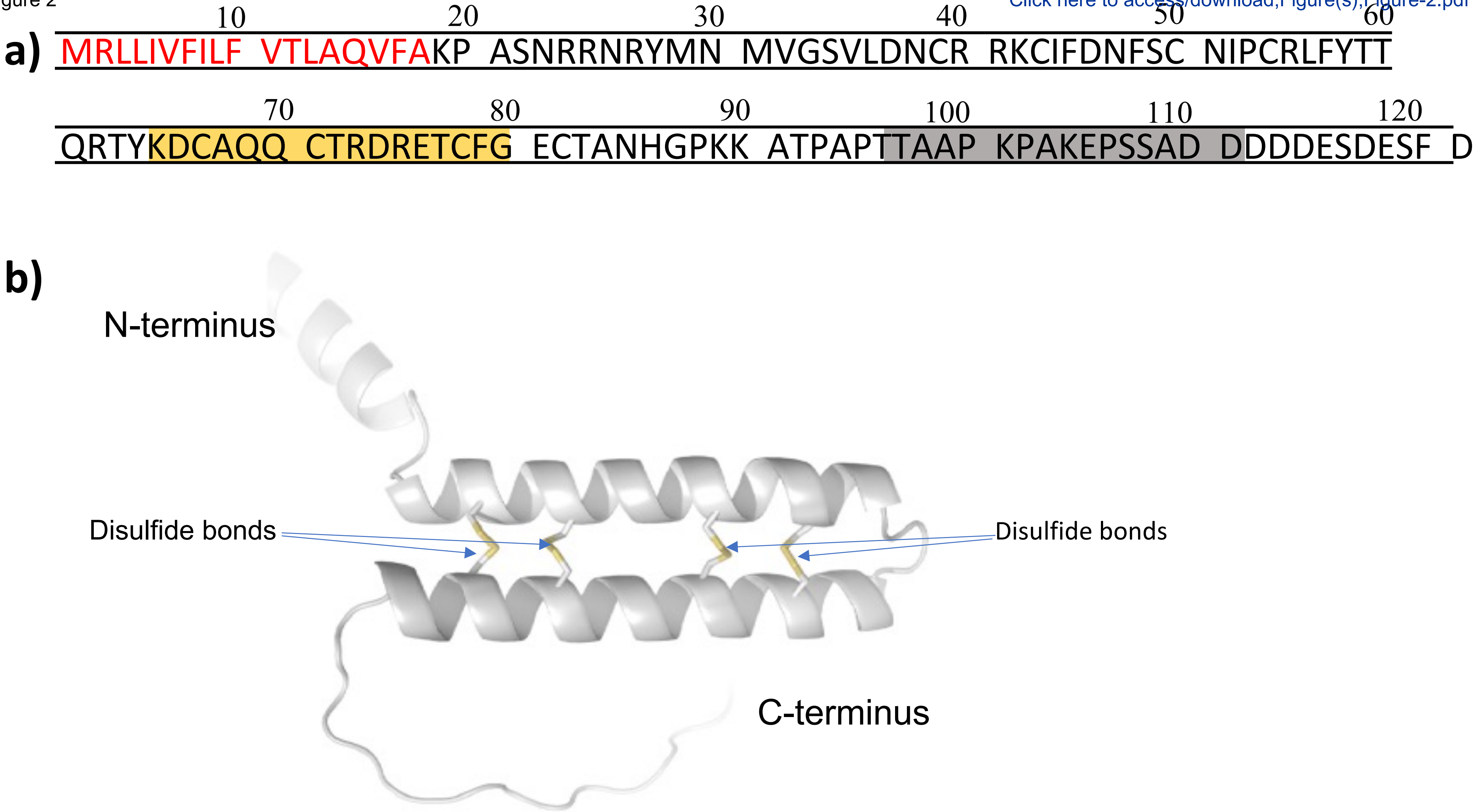
a)
10 20 30 40 50 60
MRLLIVFILF VTLAQVFAKP ASNRRNRYMN MVGSVLDNCR RKCIFDNFSC NIPCRLFYTT
70 80 90 100 110 120
QRTYKDCAQQ CTRDRETCFG ECTANHGPKK ATPAPTTAAP KPAKEPSSAD DDDDESDESF D
b)
N-terminus
Disulfide bonds
Disulfide bonds
C-terminus

Figure 3

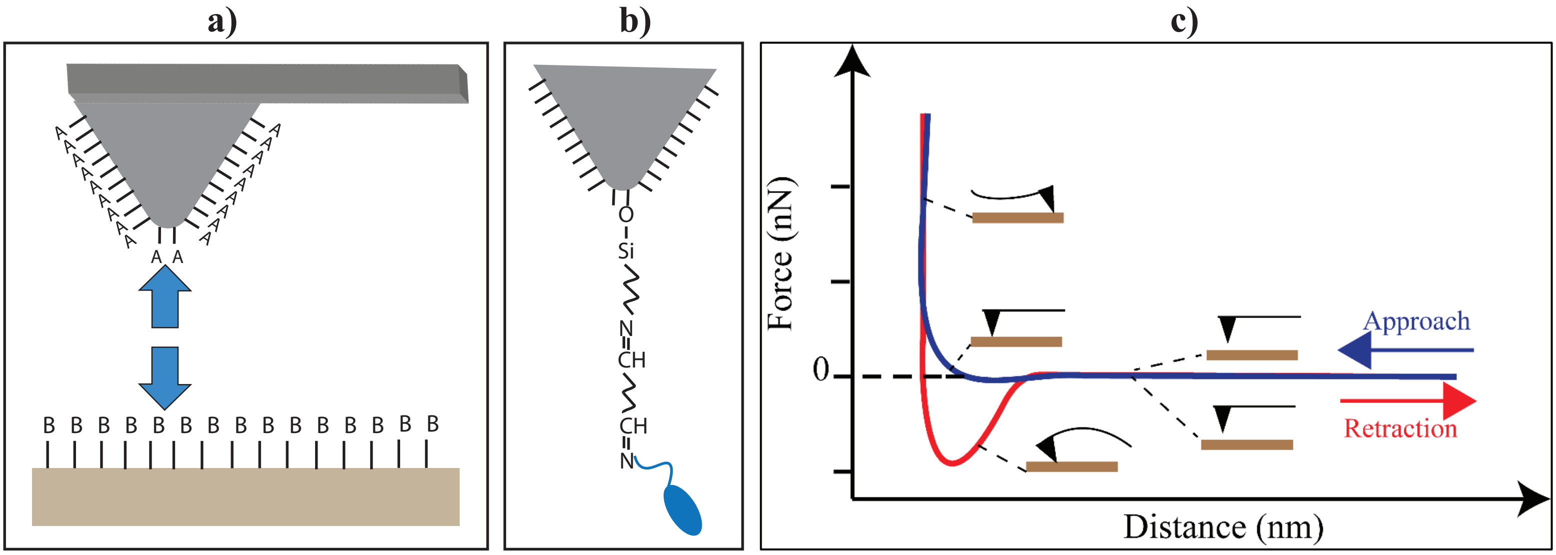
a)
A A
B B B B B B B B B B B B B B B
b)
O
Si
N
CH
CH
N
c)
Force (nN)
0
Approach
Retraction
Distance (nm)

Figure 4

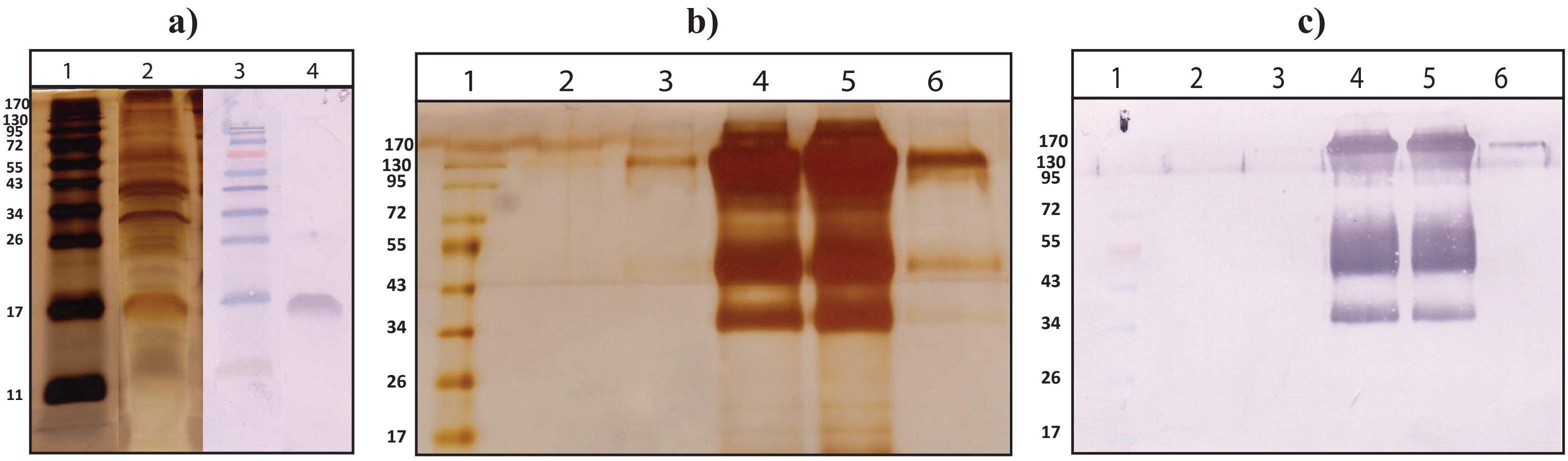
a)
1
2
3
4
170
130
95
72
55
43
34
26
17
11
b)
1
2
3
4
5
6
170
130
95
72
55
43
34
26
17
c)
1
2
3
4
5
6
170
130
95
72
55
43
34
26
17

Figure 5

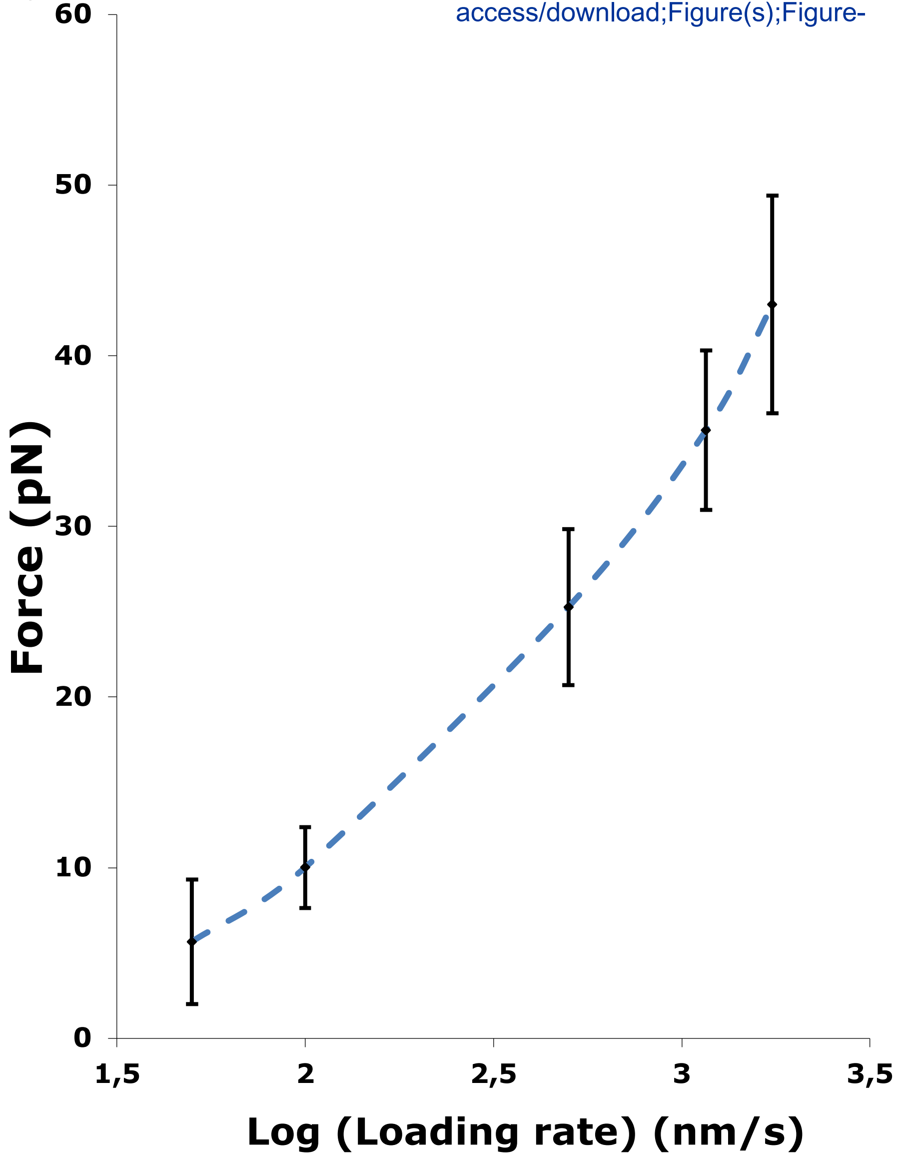

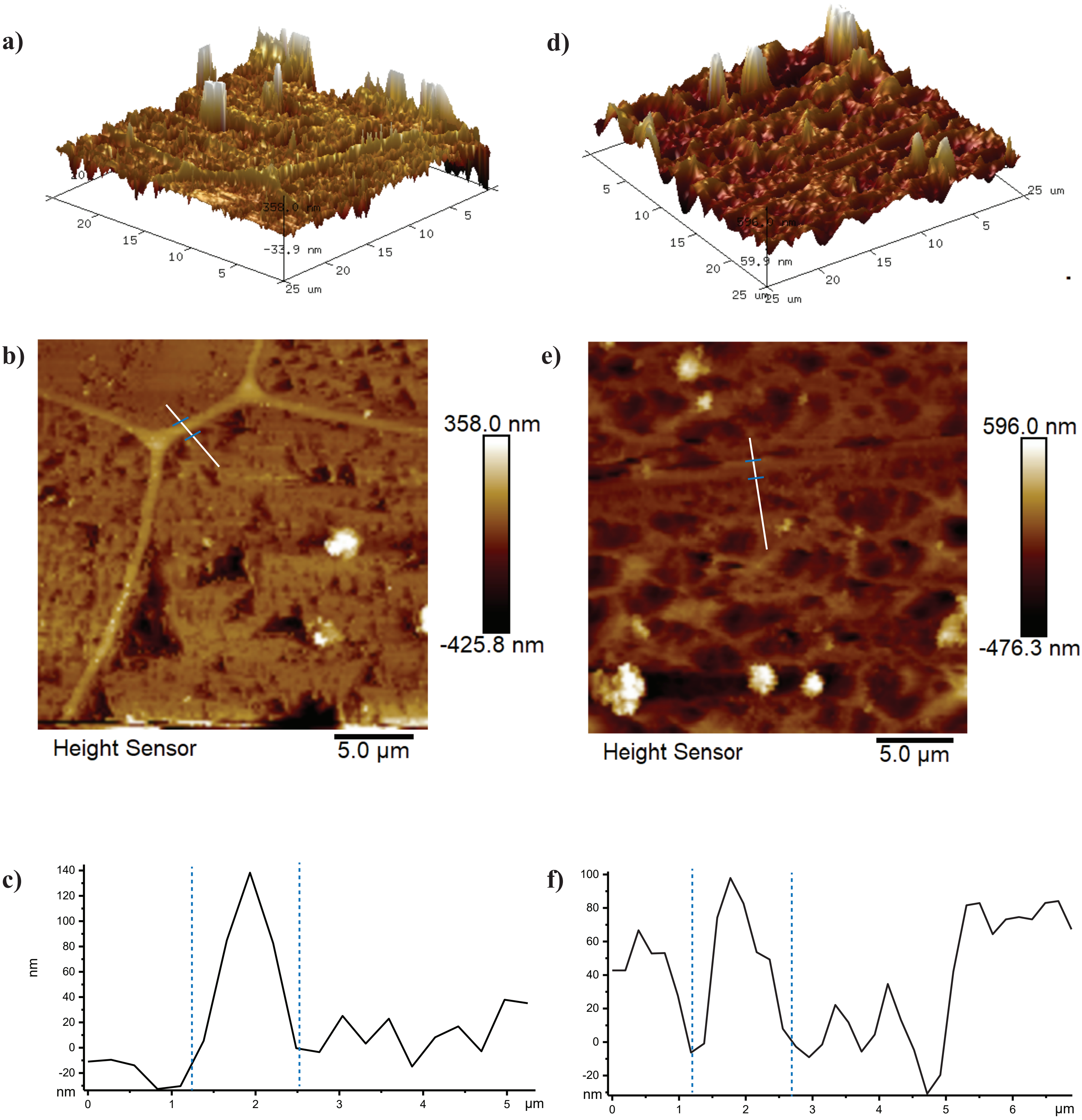
a)
358.0 nm
-33.9 nm
25 um
20
15
10
5
d)
596.0 nm
59.9 nm
25 um
b)
358.0 nm
-425.8 nm
Height Sensor
5.0 µm
e)
596.0 nm
-476.3 nm
Height Sensor
5.0 µm
c)
nm
140
120
100
80
60
40
20
0
-20
0
1
2
3
4
5
µm
f)
nm
100
80
60
40
20
0
-20
0
1
2
3
4
5
6
µm

Figure 7

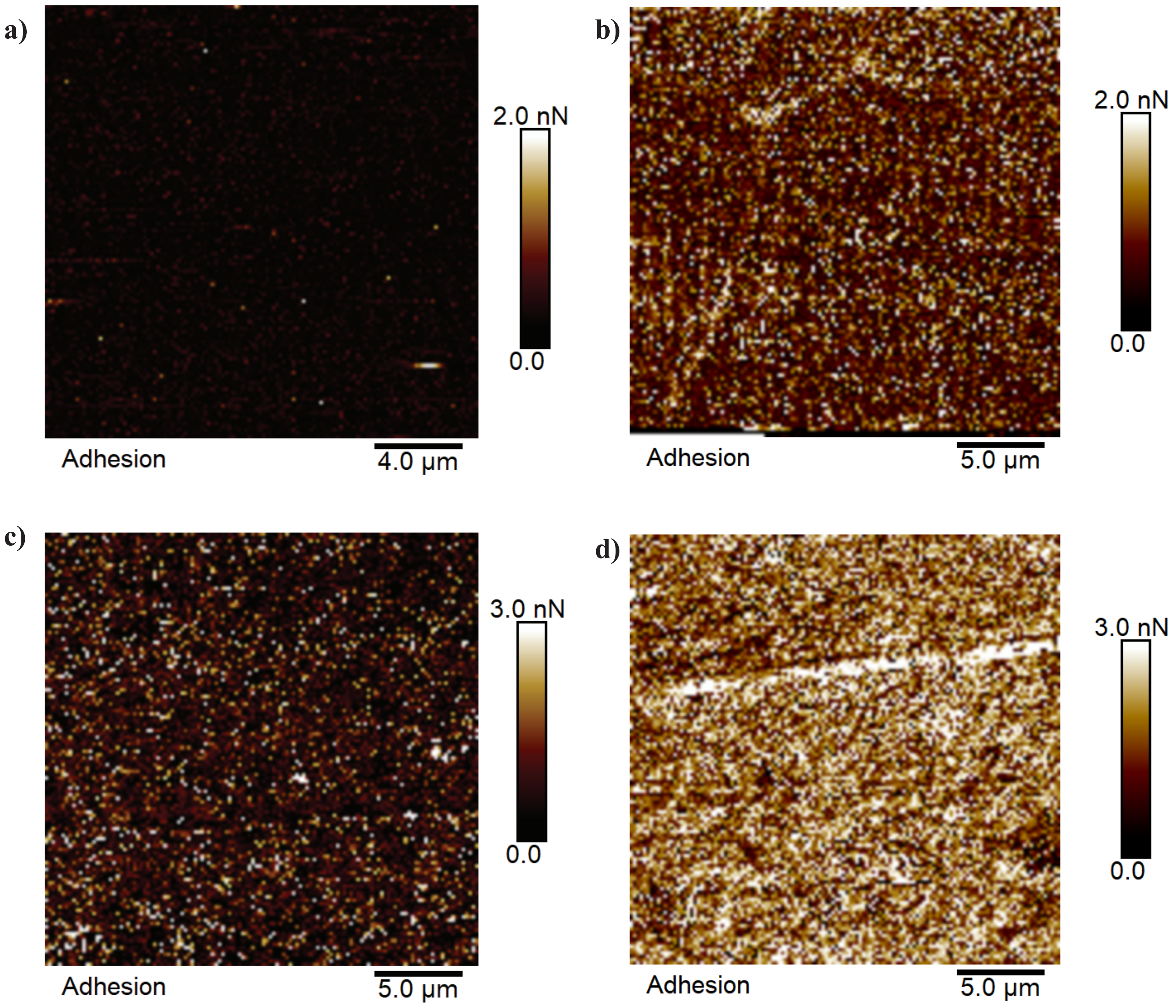
a)
2.0 nN
0.0
Adhesion
4.0 µm
b)
2.0 nN
0.0
Adhesion
5.0 µm
c)
3.0 nN
0.0
Adhesion
5.0 µm
d)
3.0 nN
0.0
Adhesion
5.0 µm

Figure 8

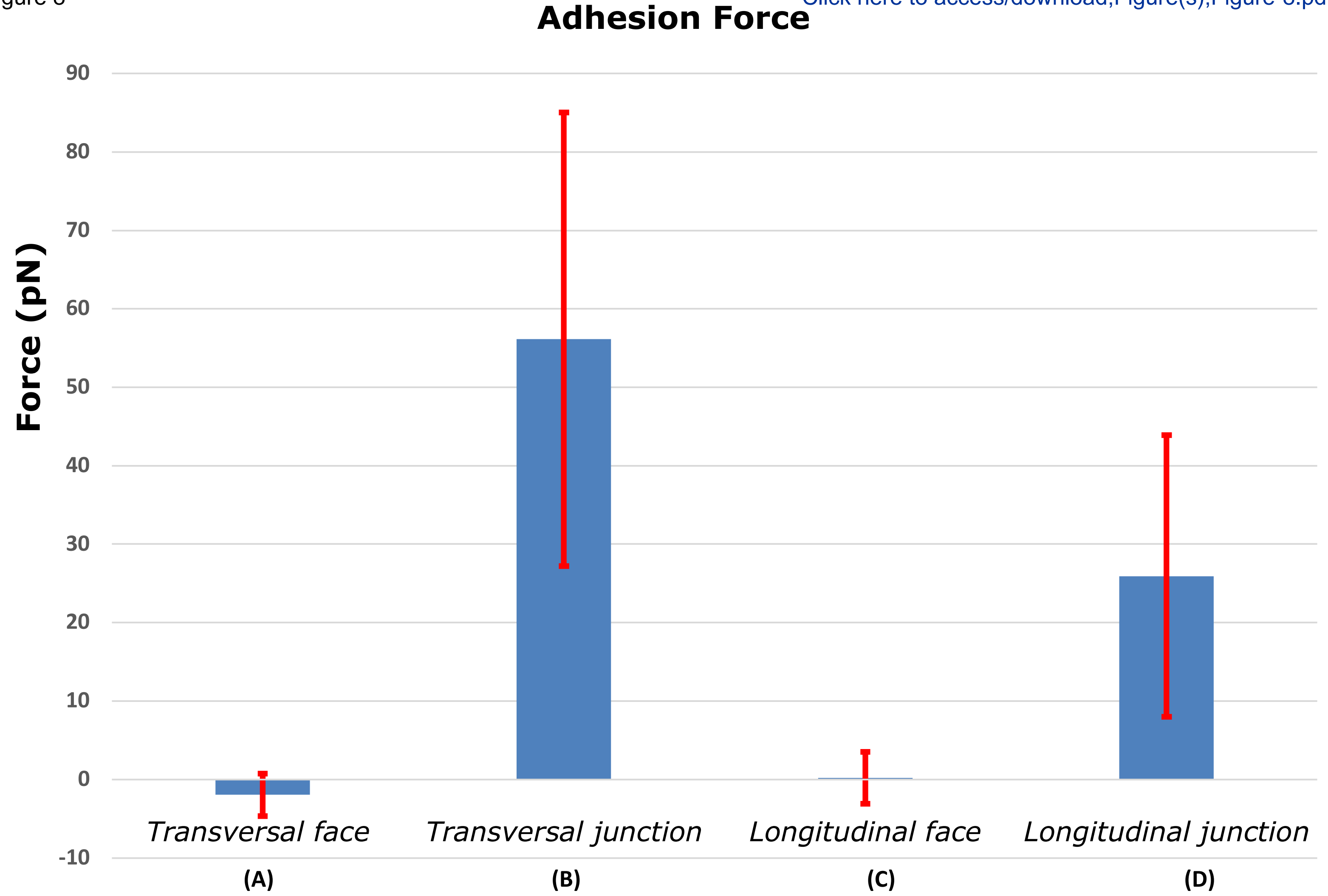
Adhesion Force
Force (pN)
90
80
70
60
50
40
30
20
10
0
-10
Transversal face
Transversal junction
Longitudinal face
Longitudinal junction
(A)
(B)
(C)
(D)

Declaration of Competing Interest

The authors declare that they have no known competing financial interests or personal relationships that could have appeared to influence the work reported in this paper.